DRAFT VERSION FEBRUARY 22, 2016
Preprint typeset using LATEX style emulateapj v. 5/2/11

FORMATION AND RECONDENSATION OF COMPLEX ORGANIC MOLECULES DURING PROTOSTELLAR LUMINOSITY OUTBURSTS

VIANNEY TAQUET[1], EVA S. WIRSTRÖM[2] AND STEVEN B. CHARNLEY[3]

(Dated: Received - ; accepted -)
Draft version February 22, 2016

ABSTRACT

During the formation of stars, the accretion of the surrounding material toward the central object is thought to undergo strong luminosity outbursts, followed by long periods of relative quiescence, even at the early stages of star formation when the protostar is still embedded in a large envelope. We investigated the gas phase formation and the recondensation of the complex organic molecules di-methyl ether and methyl formate, induced by sudden ice evaporation processes occurring during luminosity outbursts of different amplitudes in protostellar envelopes. For this purpose, we updated a gas phase chemical network forming complex organic molecules in which ammonia plays a key role. The model calculations presented here demonstrate that ion-molecule reactions alone could account for the observed presence of di-methyl ether and methyl formate in a large fraction of protostellar cores, without recourse to grain-surface chemistry, although they depend on uncertain ice abundances and gas phase reaction branching ratios. In spite of the short outburst timescales of about one hundred years, abundance ratios of the considered species with respect to methanol higher than 10% are predicted during outbursts due to their low binding energies relative to water and methanol that delay their recondensation during the cooling. Although the current luminosity of most embedded protostars would be too low to produce complex organics in hot core regions that can be observable with current sub-millimetric interferometers, previous luminosity outburst events would induce a formation of COMs in extended regions of protostellar envelopes with sizes increasing by up to one order of magnitude.

1. INTRODUCTION

Complex organic molecules (COMs) have been observed in high quantities around protostars, in their so-called high-mass hot cores and low-mass hot corinos (Blake et al. 1987; Cazaux et al. 2003; Bisschop et al. 2007). The presence of many COMs in the gas phase can be understood as due to the evaporation of ices from dust grains. In this case, atom addition reactions on grain surfaces could account for many of the organic molecules observed like CH_3OH, C_2H_5OH, CH_3CHO, or HCOOH (e.g. Herbst & van Dishoeck 2009). Other common organic molecules like di-methyl ether (DME) and methyl formate (MF) appear to require either energetic processing of simple ices containing methanol (Öberg et al. 2009) or ion-molecule reactions post-evaporation (Charnley et al. 1995). However, published astrochemical models tend to underestimate their abundances with respect to methanol, their likely parent molecule (Taquet et al. 2015). These models usually consider constant physical conditions, representative of hot cores, or simple physical models of core collapse inducing a gradual warm up of the protostellar envelope.

However, during the star formation process, accretion of the surrounding material toward the central protostar is thought to undergo frequent and strong eruptive bursts inducing sudden increases of the luminosity by one or two orders of magnitude, followed by long periods of relative quiescence. As suggested by magnetohydrodynamics (MHD) simulations, luminosity outbursts could be due to thermal, gravitational and magnetorotational instabilities (Bell & Lin 1994; Zhu et al. 2009) or gravitational fragmentation in the circumstellar disk (Vorobyov & Basu 2005; Vorobyov et al. 2015) and could explain the spread in bolometric luminosities observed for low-mass embedded protostars (see Dunham & Vorobyov 2012). FUor and EXor objects, whose SEDs can be attributed to Class I/II protostars but with heavier disks and higher accretion rates (Gramajo et al. 2014), probably undergo such luminosity outbursts (Ábrahám et al. 2004). The recent detection of an outburst toward the Class 0 protostar HOPS383 by Safron et al. (2015) suggests that luminosity outbursts are also occurring in the embedded Class 0 phase although they can be hardly observed directly, due to their optically thick surrounding envelope. The strong and sudden increase of the temperature induced by the luminosity outburst can significantly alter the chemical evolution in the envelope and in the disk by triggering the fast evaporation of solid species into the gas phase, resulting in an increase of their gaseous abundances long after the system has returned into a quiescent stage. The evaporation of icy species would therefore influence the abundances of commonly observed molecules, such as N_2H^+ and HCO^+, whose abundances are governed by CO or H_2O (Visser & Bergin 2012), an effect proposed by Jørgensen et al. (2013) to explain the non-detection of HCO^+ and the presence of CH_3OH toward the inner envelope of the low-luminosity protostar IRAS15398-3359.

The efficient ice evaporation induced by luminosity outbursts could also trigger the gas phase formation of COMs. In addition, the low binding energy of some COMs with respect to water and methanol ices would induce a differentiation in the recondensation, altering the abundances of COMs with respect to these more simple species. In this work, we investigate the hot core chemistry leading to the formation of gaseous COMs and the impact of luminosity outbursts on the

[1] Leiden Observatory, Leiden University, P.O. Box 9513, 2300-RA Leiden, The Netherlands
[2] Department of Earth and Space Sciences, Chalmers University of Technology, Onsala Space Observatory, SE-439 92 Onsala, Sweden
[3] Astrochemistry Laboratory and The Goddard Center for Astrobiology, Mailstop 691, NASA Goddard Space Flight Center, 8800 Greenbelt Road, Greenbelt, MD 20770, USA

formation and their subsequent recondensation of COMs by focusing on the formation of the two O-bearing prototype COMs di-methyl ether and methyl formate. We also compare our model predictions with results from sub-millimetric observations toward low-mass to high-mass protostars. Section 2 describes the model used in this work. Section 3 presents the chemical evolution for constant physical conditions while Section 4 shows the chemical evolution during strong and weak luminosity outbursts. We discuss the implications of this work in Section 5 and outline the conclusions in Section 6.

2. MODEL

2.1. *Physical Model*

According to hydrodynamical models of disk instability and fragmentation, the embedded Class 0 and Class I phases show a highly variable evolution of their luminosity with various outbursts of different amplitudes. In this work, we investigated how the chemical evolution is impacted by two types of outburst whose properties are taken from the model results by Vorobyov et al. (2015): 1) one strong outburst, increasing the luminosity by a factor of 100 from 2 to 200 $L_\odot$ every $\sim 0.5 - 1 \times 10^5$ yr; 2) a series of weak outbursts, increasing the luminosity by a factor of 10 only from 2 to 20 $L_\odot$, but more frequently (every $\sim 5 \times 10^3$ yr). For the two types of outburst, we assumed that the luminosity instantaneously increases from $L_{\rm min} = 2L_\odot$ to its maximal luminosity $L_{\rm max}$ and then decreases exponentially following the formula

$$L_\star(t) = (L_{\rm max} - L_{\rm min}) \exp(-t/\tau) + L_{\rm min} \quad (1)$$

τ being the outburst timescale. The outburst duration, assumed to be the time during which the luminosity remains higher than half of its maximal luminosity, is highly variable. Models and observations show that it can vary between a few decades to a few centuries depending on the type of predicted instabilities and observed source (see Audard et al. 2014). We therefore varied τ between 75 and 300 yr, $\tau = 150$ yr, corresponding to an outburst duration of ~ 100 yr, being our standard value.

Figure 1 presents the dust temperature structure in the envelope surrounding Serpens-SMM4, a typical Class 0 protostar with a current bolometric luminosity $L_{\rm bol} = 2L_\odot$ and an envelope mass of 2.1 $M_\odot$ before and during the two types of outburst considered in this work, as computed by the radiative transfer code DUSTY (Ivezic & Elitzur 1997). The protostar properties were derived by Kristensen et al. (2012) and we followed the methodology described in Taquet et al. (2014) to compute the temperature structure. Johnstone et al. (2013) found that the time needed by the dust to heat up in response to a luminosity outburst is much shorter, typically a few days to a few months, than the typical duration of a luminosity outburst. We therefore assumed that the dust temperature instantaneously scales with the luminosity evolution. From Fig. 1, it can be seen that the dust temperature roughly follows the Stefan-Boltzmann's law throughout the envelope

$$T(t) = T_{\rm min} \times (L_\star(t)/L_{\rm bol})^{1/4} \quad (2)$$

where $T_{\rm min}$ is the temperature before and at the end of the outburst. The two types of outburst expand the hot-core region, where ices are thermally evaporated at $T = 100 - 120$ K, from 15 AU to 60 AU for weak outbursts and to 150 AU for strong outbursts. We therefore considered several pre-outburst temperatures of particular interest: $T_{\rm pre} = 100$ K, which is slightly lower than the evaporation/condensation temperature of methanol; $T_{\rm pre} = 70$ K which is slightly lower than the evaporation/condensation temperature of DME and MF; and $T_{\rm pre} = 40$ K, giving $T_{\rm max} = 125$ K which is sufficient to thermally evaporate the whole content of ices. Three values of density were chosen, in order to represent the different densities expected to be found in the inner regions of Class 0 and Class I protostellar envelopes where the temperature is between 40 and 100 K (Kristensen et al. 2012): $n_{\rm H} = 5 \times 10^6, 5 \times 10^7, 5 \times 10^8$ cm^{-3}. We also adopted three values for the size of interstellar grains: $a_{\rm d} = 0.05$ μm, representing the grain size needed to match the integrated surface area observed in the diffuse ISM; $a_{\rm d} = 0.2$ μm, the upper limit of the grain size distribution observed in the diffuse ISM and commonly used by astrochemical models; and $a_{\rm d} = 1$ μm, a higher grain size obtained through grain growth in dense cores as observed by Pagani et al. (2010).

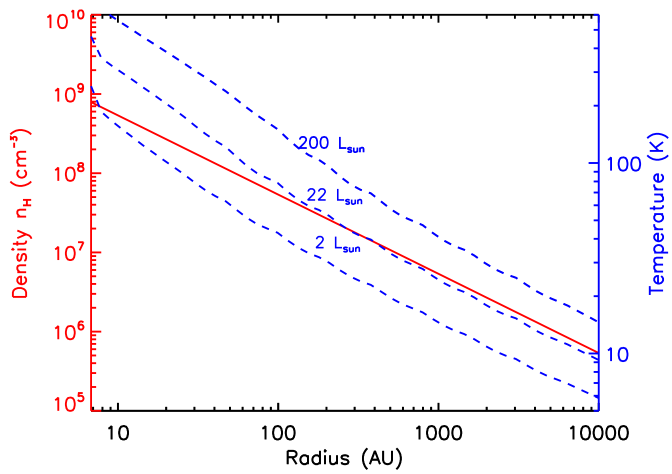

FIG. 1.— Dust temperature structure in the envelope surrounding the Class 0 protostar Serpens-SMM4, with a bolometric luminosity $L_{\rm bol} = 2L_\odot$ and an envelope mass of 2.1 $M_\odot$ before and during the two types of luminosity outburst considered in this work.

2.2. *Chemical Model*

The chemistry is followed as a function of time with the GRAINOBLE gas-grain astrochemical model presented in previous studies (Taquet et al. 2012, 2014). In this work, we focus our study on the gas phase chemistry and the gas-grain interactions through freeze-out and thermal evaporation. We used an updated version of the chemical network described in Rodgers and Charnley (2001). The rate of several key reactions has been updated while new reactions have been added following recent experimental and theoretical works. The formation of complex organics through ion-neutral gas phase chemistry is triggered by the protonation of evaporated ices, and of methanol in particular.

Electronic recombination (ER) reactions involving the protonated ions associated with methanol, formic acid, DME, and ethanol have been measured by Geppert et al. (2006); Hamberg et al. (2010a,b); Vigren et al. (2010). For the four systems, the total rate of the reaction follows the expression $k(T) \sim 10^{-6} (T/300)^{-0.7}$ cm^{-3} s^{-1} while the recombination leading to the complex organic molecule in consideration has a low branching ratio between 6 and 13 %, most of the reactions being dissociative. To our knowledge, no experimental study focusing on the ER of protonated MF has been pub-

TABLE 1
INITIAL ABUNDANCE, BINDING ENERGY, AND PROTON AFFINITY OF SELECTED SPECIES.

Species	$n_{\rm ini}/n_{\rm H}$	$E_{b,\rm bare}$ (K)	$E_{b,\rm wat}$ (K)	$E_{b,\rm pure}$ (K)	Ref. (E_b)	PA[1] (kJ/mol)
H_2O	1×10^{-4}	1870	5775	5775	2, 3	689
CO	3.8×10^{-5}	830	1150	855	4, 5, 6	593
N_2	1.6×10^{-5}	790	790	790	7	494
CO_2	3.0×10^{-5}	2270	2690	2270	5, 8	539
CH_4	5.0×10^{-6}	1090	1090	1090	9	544
NH_3	5.0×10^{-6}	5535	5535	3075	4, 10	854
H_2CO	2.5×10^{-6}	3260	3260	3765	11	713
CH_3OH	7.0×10^{-6}	5530	5530	4930	4, 12	754
HCOOH	1.6×10^{-6}	5570	5570	5000	4, 13	743
C_2H_5OH	1.6×10^{-6}	6795	6795	5200	14, 13	776
CH_3OCH_3	0	4230	4230	3300	14, 13	792
CH_3OCHO	0	4630	4630	4000	14, 13	782
C_2H_5OCHO	0	5895	5895	4900	15	799
$CH_3OC_2H_5$	0	5495	5495	4400	16	809
$C_2H_5OC_2H_5$	0	6760	6760	5100	17	828
CH_3CN	0	4680	4680	4680	14, 13	781

NOTE. — [1]: The proton affinities (PA) are taken from the NIST Chemistry WebBook (http://webbook.nist.gov/chemistry/) [2]: Avgul & Kiselev (1970); [3]: Fraser et al. (2001); [4]: Collings et al. (2004); [5]: Noble et al. (2012a); [6]: Acharyya et al. (2007); [7]: Bisschop et al. (2006); [8]: Sandford & Allamandola (1990); [9]: Herrero et al. (2010); [10]: Sandford & Allamandola (1993); [11]: Noble et al. (2012b); [12]: Brown & Bolina (2009); [13]: Öberg et al. (2009); [14]: Lattelais et al. (2011); [15]: E_b = E_b(CH_3OCHO) + E_b(C_2H_5OH) - E_b(CH_3OH); [16]: E_b = E_b(CH_3OCHO_3) + E_b(C_2H_5OH) - E_b(CH_3OH); [17]: E_b = E_b(CH_3OCHO_3) + 2× (E_b(C_2H_5OH) - E_b(CH_3OH))

lished so far. We assumed the same rate and branching ratio as for the ER of protonated DME measured by Hamberg et al. (2010a).

As in Rodgers and Charnley (2001), we included proton transfer (PT) reactions involving major ice species and abundant complex organics listed in Table 1 if they are thought to be exothermic. The exothermicity of the PT reaction

$$\mathrm{AH^+ + B \rightarrow A + BH^+} \qquad (3)$$

is given by the difference of proton affinities (PA) of B and A. The reaction will therefore occur if the proton affinity of B is higher than that of A. Table 1 lists the proton affinity of the major ice species and relevant complex organics. In particular, ammonia NH_3 easily reacts with most protonated ions through exothermic barrierless PT reactions due to its high proton affinity. PT reactions can be in competition with charge transfer and condensation reactions (see Huntress 1977) while dissociative proton transfer can occur when the PA of the acceptor greatly exceeds that of the donor, but the dissociation can only on the acceptor molecule (see Smith et al. 1994). Hemsworth et al. (1974) experimentally studied at 297 K the reactivity of 11 reactions between ammonia and the protonated counterpart of neutral molecules with lower PA and of different complexity, from H_2 to C_4H_8. They showed that all the studied reactions led to non-dissociative PT reactions, the formation of NH_4^+ appearing to be the dominant ($\geq$ 90 %) channel in each case, which occur at the collisional rate of $\sim 2 \pm 1 \times 10^{-9}$ cm^3 s^{-1}. In a latter study, Feng & Lifshitz (1994) experimentally studied reactions involving protonated formic acid and 11 neutral complex organic molecules of higher proton affinities, such as methanol, methyl cyanide, acetone and even more complex species like dimethyoxyethane $CH_3OCH_2CH_2OCH_3$. All the reactions were also found to be non-dissociative ($\geq$ 99 %) proton-transfer reactions occurring at the collisional rate $\sim 2{\pm}1{\times}10^{-9}$ cm^3 s^{-1} (see Anicich 1993, for a more exhaustive list of experimentally studied PT reactions). Following these experimental results, we assumed that all the PT reactions introduced in the chemical network are non-dissociative and occur with a rate of 2×10^{-9} cm^3 s^{-1}.

Experiments and quantum calculations show that that the reaction between $CH_3OH_2^+$ and H_2CO does not lead to protonated methyl formate (Karpas & Mautner 1989; Horn et al. 2004). In this model, protonated methyl formate is instead formed through the barrierless methyl cation transfer reaction (Ehrenfreund & Charnley 2000)

$$\mathrm{CH_3OH_2^+ + HCOOH \rightarrow HC(OH)OCH_3^+ + H_2O}. \qquad (4)$$

Experimental and theoretical studies of this reaction system indicate that the *trans* conformer of protonated methyl formate should be produced and that the channel forming the more excited *cis* conformer of protonated MF has an activation barrier of 1320 K (Neill et al. 2011; Cole et al. 2012). The rate of this reaction has been measured experimentally by Cole et al. (2012) who measured a predominant branching ratio of 95 % for adduct ion products and a low branching ratio of 5 % for the reaction leading to protonated MF. However, Cole et al. (2012) suggested that the branching ratio for the adduct ion would be lowered in the ISM due to the lower pressures found in the ISM with respect to the pressure obtained at the lab. We therefore assumed a branching ratio of 100 % for the reaction leading to $\mathrm{HC(OH)OCH_3^+}$. According to the proton affinities of (*cis*-)MF and NH_3, the PT reaction between *cis*-protonated MF and NH_3 is barrierless and has a high exothermicity of $\sim$ 70 kJ/mol (see Table 1). The energy difference between the *cis*- and *trans*-protonated MF conformers is only about 25 kJ/mol (Neill et al. 2011), the reaction between *trans*-protonated MF and NH_3, forming either *cis*-MF or *trans*-MF, is therefore also likely exothermic. Since there are, to our knowledge, no quantitative data on the branching ratios for the formation of *cis*- or *trans*-MF via this reaction, we assumed a branching ratio of 100 % for the formation of the more stable *cis*-MF conformer, which is more stable than the *trans*- conformer by 25 kJ/mol. The gas phase chemistry forming other O-bearing complex organic molecules from the evaporation of methanol and ethanol is summarized in Figure 2, and follows the experimental results of Karpas & Mautner (1989) (see also Charnley et al. 1995). Dimethyl ether, methyl ethyl ether, and diethyl ether are formed from reactions between protonated methanol or protonated ethanol with methanol or ethanol. We assumed that the reaction between protonated ethanol and formic acid, forming protonated ethyl formate, has the same rate than the reaction between methanol and formic acid. In total, the chemical network consists in 325 species and 2787 chemical processes.

2.3. *Initial Abundances and Binding Energies*

For each species i, the effective binding energy $E_b(i)$ relative to the surface is given by the additive contribution of the binding energy relative to a bare grain substrate, an Amorphous Solid Water (ASW), and a pure ice i according to their fractional coverage in the ice, following the methodology described in Taquet et al. (2014). The binding energies of the main ice components and some abundant COMs with respect to the three substrates have been measured in laboratory experiments and are listed in Table 1. Differences in the binding

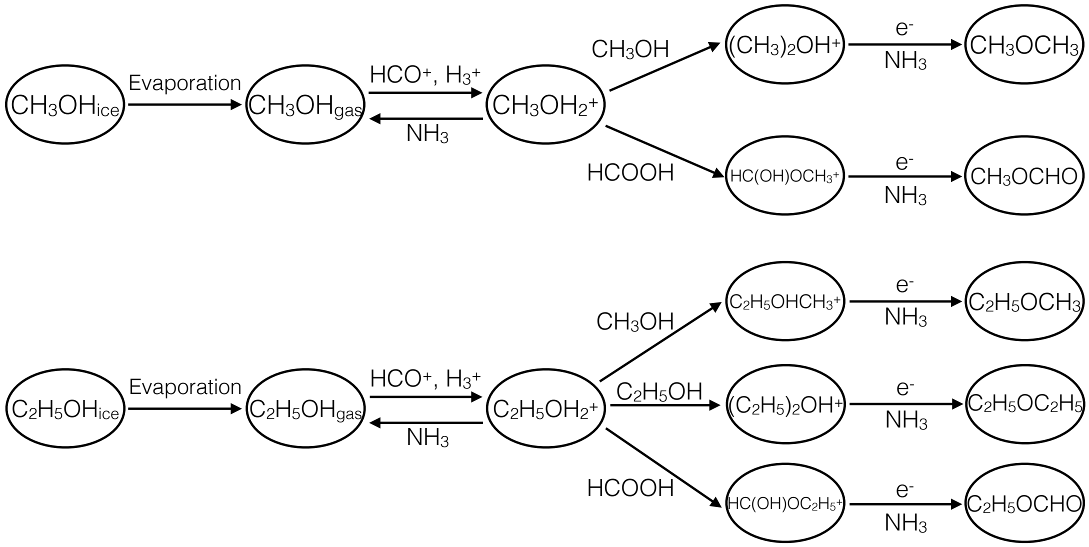

FIG. 2.— Schematic picture of the gas phase chemical network used in this work to produce the complex organic molecules dimethyl ether, methyl formate, methyl ethyl ether, diethyl ether and ethyl formate from the evaporation of methanol and ethanol.

energies of complex organics can be noticed, leading to different temperatures of sublimation and recondensation. For example, as MF and DME show lower binding energies than methanol, they will evaporate and recondense at lower temperatures of 70-80 K with respect to methanol, but also to formic acid or water, which recondense at 100-110 K. In contrast, ethanol C_2H_5OH has a higher binding energy and evaporates at a higher temperature of 120 K.

The initial abundances of molecular ices are taken from infrared observations of ices and are listed in Table 1. The water abundance of 10^{-4} with respect to H nuclei follows ice observations by Tielens et al. (1991) and Pontoppidan et al. (2004). Abundances of solid CO, CO_2, CH_4, NH_3, and CH_3OH are taken from the abundance medians derived by Öberg et al. (2011) toward a sample of protostars. Theoretical models suggest that H_2CO, HCOOH, and C_2H_5OH should also be present in cold interstellar ices (see Herbst & van Dishoeck 2009). However, their abundances in ices are highly uncertain since the features used for their detection are contaminated by other mixtures. We fixed the H_2CO abundance to 2.5 %, following the abundance of the C1 component attributed to H_2CO+HCOOH. The HCOOH abundance has been derived from the band feature at 7.25 μm detected by Boogert et al. (2008) toward 12 low-mass protostars, giving a mean abundance of 3.2 % with respect to water. However, C_2H_5OH appears to be a plausible carrier for this feature as well (see Öberg et al. 2011). We therefore assumed an abundance of 1.6 % for HCOOH and C_2H_5OH.

3. CHEMISTRY DURING CONSTANT PHYSICAL CONDITIONS

3.1. *Impact of proton transfer reactions*

We show in Figure 3 the impact of the proton transfer reactions involving NH_3 introduced in the chemical network on the formation and destruction of COMs for constant physical conditions: $n_{\rm H} = 5 \times 10^7$ cm^{-3}, $T = 150$ K, $\zeta = 3 \times 10^{-17}$ s^{-1}, $A_{\rm V} = 20$ mag, assumed to be our standard physical parameters.

After their evaporation into the gas phase, ice species, such as CH_3OH, HCOOH, C_2H_5OH, are protonated through proton-transfer reactions involving the abundant ions H_3O^+ or HCO^+. $CH_3OH_2^+$ can then react with CH_3OH, or HCOOH via methyl cation transfer reactions to form the DME and MF protonated ions. Since the ER reactions involving the protonated COM ions lead predominantly to their break-up into small molecules, complex organics are not formed efficiently through gas phase chemistry if PT reactions involving NH_3 are neglected, their abundances not exceeding 10^{-8}. Moreover, they are quickly destroyed in less than a few 10^4 yr into small fragments. The incorporation of the PT reactions involving NH_3 increases the COM abundances by one to two orders of magnitude. PT reactions, which are likely non-dissociative, also delay the destruction of COMs since they dominate over the dissociative ER reactions. DME and MF reach an abundance peak of 5×10^{-7} and 2×10^{-7} in $2{-}3 \times 10^4$ yr, respectively and start to be efficiently destroyed after 5×10^4 yr. MF reaches a slightly lower abundance than DME due to the lower abundance of HCOOH relative to CH_3OH. A similar chemistry triggered by the protonation of ethanol produces methyl ethyl ether, di-ethyl ether and ethyl formate as depicted in Fig. 2 (see also Charnley et al. 1995). As seen in Table 1 ethanol has a higher proton affinity than methanol. The PT reaction between protonated methanol and neutral ethanol therefore enhances the ethanol protonation with respect to methanol and induces a more efficient conversion from ethanol to the longer COMs, like ethyl formate, methyl ethyl ether or di-ethyl ether. Their abundance remains nevertheless lower than MF and DME because of the lower initial abundance of ethanol.

The incorporation of the new PT reactions also tends to enhance the destruction of NH_3 as protonated methanol becomes the main proton donor of NH_3. However, NH_3 survives for a longer time than other more complex species because the ER reaction involving NH_4^+ is mostly non-dissociative and reforms either NH_3 or NH_2. Moreover, NH_2 can also be protonated to form NH_3^+ that reforms NH_3 through the reaction between NH_3^+ and H_2. Since this latter process is in competition with the reaction between NH_2 and H, whose rate increases with the temperature, higher temperatures tend to increase the destruction efficiency of ammonia. Our gas phase chemical network also produces methyl cyanide CH_3CN, from the reaction between HCN and CH_3^+ through protonated methyl cyanide but in lower abundances ($\sim 10^{-8}$) and obtained in a

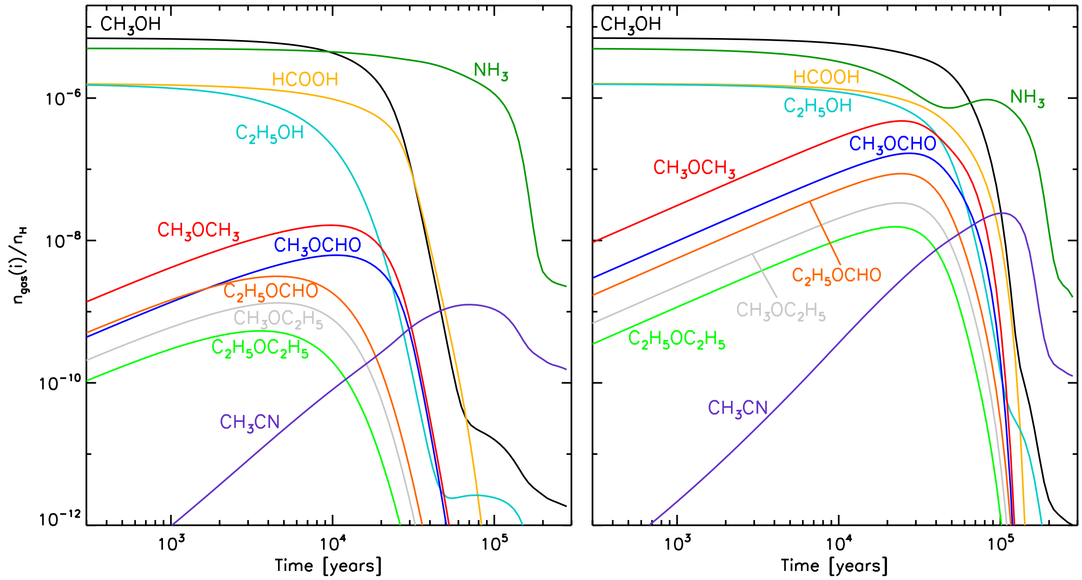

FIG. 3.— Temporal evolution of the absolute abundances of complex organics by neglecting (left) and including (right) the proton transfer reactions with ammonia for $n_{\rm H} = 5 \times 10^7$ cm^{-3}, $T = 150$ K, $\zeta = 3 \times 10^{-17}$ s^{-1}, $A_{\rm V} = 20$ mag.

longer time ($\sim 10^5$ yr).

3.2. *Impact of other parameters*

In order to compare our model predictions to observations of complex organics toward protostars, we show in Figure 4 the evolution of the predicted abundances of formic acid, ethanol, DME, MF, ethyl formate, and methyl ethyl-ether with respect to methanol as a function of the absolute methanol abundance for different values of the total density, and temperature.

With time, the abundance ratios evolve from the right to the left of each panel, their exact evolution depending on the initial abundance in ices and their chemistry in the gas phase. Formic acid and ethanol both have an initial abundance of $\sim$ 20 % with respect to methanol according to the standard assumed abundances (see Table 1). The temporal evolution of their abundance, however, shows opposite trends because of their different proton affinities. Ethanol has a higher proton affinity than methanol, allowing the proton-transfer reaction between protonated methanol and ethanol to occur. The protonation of ethanol and its conversion to larger species will therefore be enhanced with respect to methanol. Its abundance ratio therefore decreases to $\sim$ 1 % for the standard model (solid lines in Fig. 4). On the other hand, formic acid has a lower proton affinity than methanol, methanol will consequently limit its protonation through the proton transfer reaction between protonated formic acid methanol and therefore its destruction to larger species. Its abundance remains constant for a longer time than methanol, its abundance ratio slightly increasing from $\sim$ 20 to $\sim$ 50 %. Gas phase chemistry produces high abundance ratios of MF and DME, reaching peaks of 10 and 4 % respectively at $2 - 3 \times 10^4$ yr when the methanol abundance is still high ($> 10^{-6}$). The dissociative ER reactions involving the protonated COMs have slightly higher rates than the ER reactions destroying protonated methanol (1.8×10^{-6} for DME vs 0.9×10^{-6} cm^{-3} s^{-1} for methanol at 300 K), the MF and DME abundance ratios therefore slowly decrease with the destruction of methanol and other large molecules at longer timescales. Abundance ratios of ethyl formate and methyl ethyl ether show similar trends than MF and DME but are lowered by one order of magnitude, due to the lower initial abundance of ethanol.

The abundance ratios also depend on the assumed physical conditions. The density slightly influences the efficiency of the COMs formation since an increase of density from 5×10^6 to 5×10^8 cm^{-3} slightly increases the MF and DME abundances, but only by a factor of 4 at maximum, due to the decrease of the abundance of electrons and protonated ions that destroy neutral COMs. The abundance of COMs does not depend on the temperature for values lower than 150 K, their abundances only varying by a factor of 2 at maximum. However, higher temperatures enhance the destruction of COMs, decreasing the MF and DME abundance ratios by one order of magnitude between 150 and 200 K due to the more efficient destruction of NH_3, as explained in section 3.1.

However, the most important parameter is the initial abundance of ammonia injected in the gas phase as it governs the efficiency of proton exchange reactions both with $CH_3OH_2^+$ and with protonated COM ions. Figure 5 shows the maximal abundance relative to methanol reached by DME, MF, ethyl formate, and methyl ethyl ether and the time required to reach their maximal abundances as function of the initial abundance of ammonia. On the one hand, a low NH_3 abundance induces an efficient protonation of methanol but also a low formation of COMs from large ions, possibly mostly by ERs. On the other hand, a very high NH_3 abundance keeps the protonated methanol at such low levels that both the destruction of methanol by dissociative electron recombination, and the formation of COMs, are limited (Rodgers and Charnley 2001). Consequently, abundances of COMs increase with ammonia abundances between X(NH_3)/X(H_2O) = 0 % and 20 % with respect to water to reach peaks of 30 and 8 % for DME and MF, respectively and then decline for higher ammonia abundances. However, the time needed to reach the maximal abundances strongly increases with the initial ammonia abundance because it delays the protonation of methanol. A reasonable amount of solid NH_3, with similar abundances to those measured in interstellar ices toward low-mass protostars (X(NH_3)/X(H_2O) = 5 - 10 %), provides the best balance between efficient methanol protonation and efficient formation

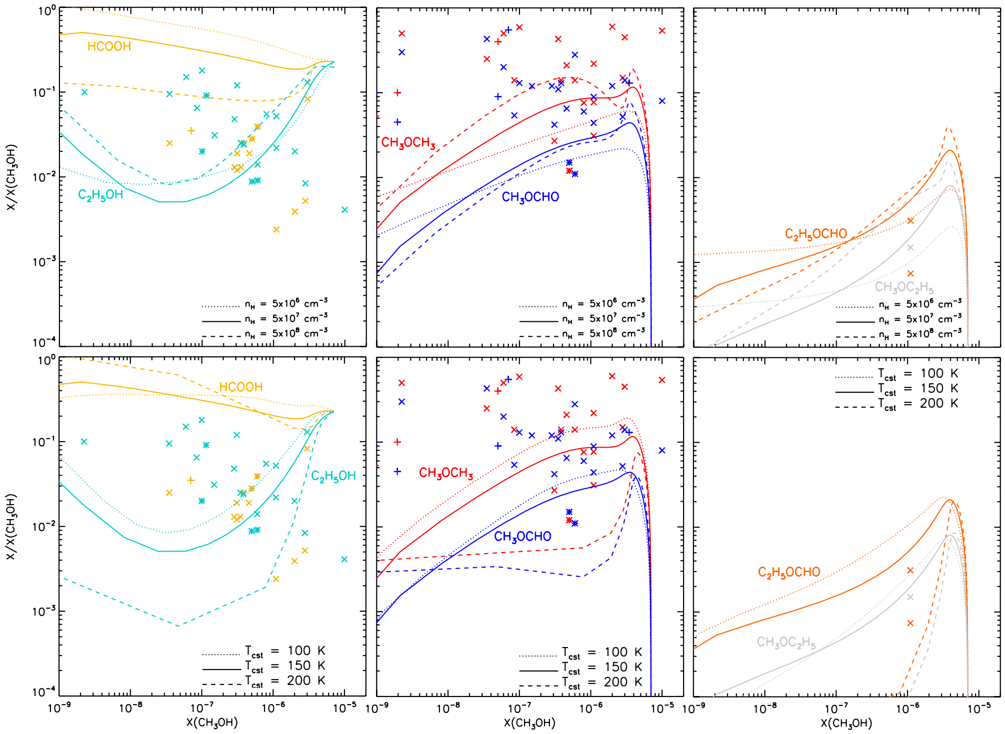

FIG. 4.— Evolution of the gaseous abundances of formic acid, ethanol (left panels), di-methyl ether, methyl formate (center panels), ethyl formate and methyl ethyl ether (right panels) relative to methanol with the absolute CH_3OH abundance assuming constant physical conditions. Top and bottom panels show the effect of the density n_H, and the temperature T_{cst}, respectively, on the chemistry. Pluses, stars, and crosses represent the ratios observed toward low-mass, intermediate-mass, and high-mass protostars, respectively, summarised in Taquet et al. (2015).

of neutral COMs from protonated ions, enhancing the gas phase production of O-bearing COMs. On the other hand, a high initial abundance of solid ammonia of 25 %, as assumed by Rodgers and Charnley (2001), inhibits the conversion of methanol and ethanol to more complex species as it requires too much time (4×10^5 yr compared to the Class 0 lifetime of $\sim 10^5$ yr Evans et al. 2009).

Infrared observations of interstellar ices suggest that solid methanol shows a strong variation of its abundance, from less than 3 % in a significant number of low-mass protostars to more than 30 % in a few massive sources (Gibb et al. 2004; Bottinelli et al. 2010; Öberg et al. 2011). Although the origin of the 7.25 μm band is still a matter of debate, HCOOH abundances derived from observations of this band toward low- and high-mass protostars is also highly variable, between less than 0.5 % to more than 7 %. The gas phase abundance of the COMs studied in this work obviously depends on the initial abundance of solid species injected in the gas phase. The maximal abundance ratios reached by the daughter COMs depend on the ratio between the initial methanol (or ethanol) abundance relative to ammonia. A low methanol abundance relative to NH_3 limits its protonation due to the high NH_3 abundance that reforms back methanol while gas phase chemistry is not efficient enough to produce a high abundant of COMs when the methanol abundance is higher. It is found that DME and MF abundance ratios reach their maximum when methanol and ammonia have a similar abundance of 5-10 %.

4. CHEMICAL EVOLUTION DURING LUMINOSITY OUTBURSTS

4.1. *Strong luminosity outbursts*

This section describes the chemical evolution induced by one strong luminosity outburst, in which the central luminosity increases from 2 to 200 $L_\odot$, inducing an increase of the temperature by a factor of ~ 3.2, as explained in section 2.1. The chemical evolution occurring during luminosity outbursts strongly depends on the binding energy of neutral species. We will therefore focus our study on di-methyl ether and methyl formate whose binding energies have been comprehensively studied experimentally by different groups, in contrast to the

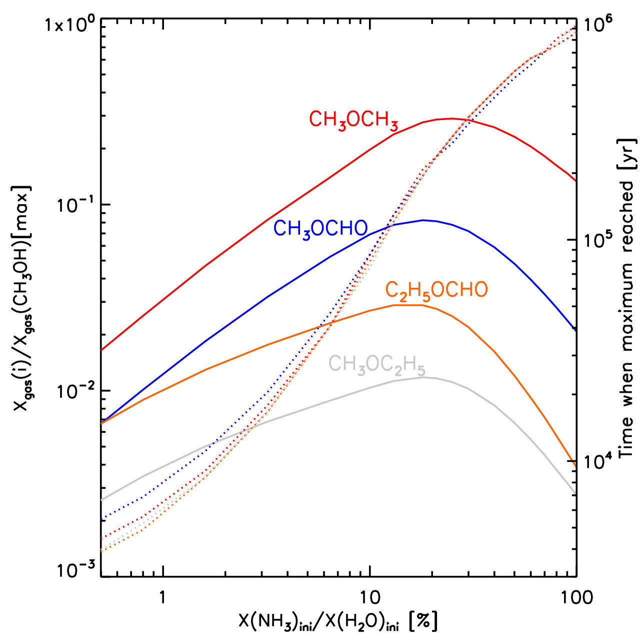

FIG. 5.— Maximum di-methyl ether, methyl formate, ethyl formate, and methyl ethyl ether abundances relative to methanol (solid lines) and time when the maximum is reached (dotted lines) as a function of the initial abundance of ammonia.

heavier species ethyl formate, methyl ethyl ether or di-ethyl ether whose binding energies are guessed values. The sudden increase in temperature induced by the luminosity outburst triggers the evaporation of all icy species into the gas phase, allowing an efficient formation of daughter COMs, such as DME and MF, through the gas phase chemistry described in the previous section.

Figure 6 presents the temporal evolution of abundances of complex organics during one strong luminosity outburst. In all panels, the solid curves show the chemical evolution during the model using the standard parameters ($n_{\rm H} = 5 \times 10^7$ cm^{-3}, $T_{\rm min} = 70$ K, $\tau = 150$ yr, $a_{\rm d} = 0.2$ μm). The dashed and dotted curves show the chemical evolution where one parameter is varied at a time. The formation of COMs is efficient but limited by the short timescale of the outburst and the fast decrease of the temperature that induces a rapid recondensation of neutral species, and of methanol in particular Absolute abundances reached during outbursts are consequently lower than those obtained for constant physical conditions. DME and MF reach abundance peaks of $\sim 10^{-8}$ only, the exact value of the maximal abundance depending on the assumed physical parameters. The absolute abundances of COMs tend to increase with the pre-outburst temperature and the outburst timescale, since they directly affect the time spent by ices in the gas phase before their recondensation during the cooling. The increase of the poorly constrained luminosity outburst timescale from 75 to 300 yr or the pre-outburst temperature from 40 to 100 K increases the DME and MF abundancess by one order of magnitude simply due to the delay of the recondensation of neutral species.

As shown in Table 1, MF and DME have lower binding energies than methanol by ~ 1000 K, inducing a difference of 20-30 K in their temperature of recondensation. Methanol starts to condense at $100 - 110$ K whereas MF and DME freeze-out at a lower temperature of $70 - 80$ K. The impact of the binding energy differences is illustrated in the bottom panels of Fig. 6, showing the evolution of the DME and MF abundances with respect to methanol as function of the methanol abundance. The formation efficiency of COMs is limited by the short luminosity outburst timescales, inducing low abundance ratios at high methanol abundances. However, the low binding energy of COMs delays their freeze-out with respect to methanol. If the outburst timescale is longer than the freeze-out timescale, given by this formula

$$\tau_{\rm fr} = 100 \text{ yr} \, \frac{5 \times 10^7 \text{ cm}^{-3}}{n_{\rm H}} \frac{a_{\rm d}}{0.2 \, \mu\text{m}}, \quad (5)$$

then the methanol abundance efficiently decreases during the cooling before the onset of the recondensation of the more volatile DME and MF, increasing their abundance ratio. As a consequence, the evolution of the abundance ratio of COMs also strongly depends on the total density of H nuclei and the grain size. Higher densities or smaller grain sizes increase the freeze-out rate of neutral species like methanol. This induces a slight decrease of absolute abundances of COMs because methanol spends slightly less time in the gas phase but, more importantly, a strong increase of their abundance ratios by more than one order of magnitude as soon as the freeze-out timescale becomes shorter than the outburst timescale. According to equation (5), a high density of 5×10^8 cm^{-3} or a small grain size of 0.05 μm decrease the freeze-out timescale to less than a few decades, inducing an efficient depletion of methanol, with abundances down to 10^{-8}, before the onset of the MF and DME recondensations at $70 - 80$ K. Abundance ratios of 100 % and 10 % can thus be reached for DME and MF, respectively when the methanol abundance is still higher than 10^{-8}.

4.2. *Weak and frequent luminosity outbursts*

Given the lifetime of Class 0 protostars ($\sim 10^5$ yr; Evans et al. 2009), the dynamical timescale of the material in the envelope inside the centrifugal radius ($10^4 - 10^5$ yr; Visser et al. 2009), and the expected frequency of weak outbursts, increasing the luminosity by one order of magnitude, of $\sim 5 \times 10^3 - 10^4$ yr (Scholz et al. 2013; Vorobyov et al. 2015), it is likely that cells of material located outside the water snowline undergo several processes of ice evaporation and condensation. According to Fig. 1, such luminosity outbursts are likely strong enough to trigger the evaporation of the whole ice content into the gas phase up to radii showing a pre-outburst temperature lower than the condensation temperature of MF and DME (75 K).

Figure 7 shows the evolution of the absolute abundances and the abundance ratios during a series of 10 weak outbursts, in which the temperature is increased from 70 to 125 K induced by a luminosity increase of one order of magnitude, occurring every 5×10^3 yr. As for the strong luminosity outburst case, three values of density were chosen, in order to represent the spread of density expected to be found at radii where $T = 70$ K in Class 0 and Class I protostars. The abundance of MF and DME formed through gas phase chemistry gradually increases with the outburst number up to one order of magnitude after 5 outbursts. However, MF and DME are not efficiently produced during subsequent outbursts because of the gradual destruction of ammonia during outbursts allowed by the longer total timescale (5×10^4 yr) and its low binding energy that prevents it to freeze-out. After five outbursts, the ammonia abundance is already lower than 10^{-6} or 1 % with respect to water, preventing an efficient formation of COMs from protonated ions through proton-transfer reactions (see Fig. 5).

It can also be seen that the formation efficiency of COMs decreases more strongly with the density with respect to the strong luminosity outburst case. The abundances of MF and DME reached after 5 outbursts decrease by one order of magnitude from 10^{-7} to 10^{-8} between $n_{\rm H} = 5 \times 10^6$ and $n_{\rm H} = 5 \times 10^8$ cm^{-3}. This is due to the very short time spent by CH_3OH in the gas phase at high densities during each weak outburst. In total, the CH_3OH abundance remains higher than 10^{-6} for more than 10^4 yr at $n_{\rm H} = 5 \times 10^6$ cm^{-3} but only for 400 yr at $n_{\rm H} = 5 \times 10^8$ cm^{-3}, a shorter timescale by a factor of 20. In contrast, during one strong luminosity outburst, CH_3OH abundances can remain high for 200 and 1000 yr at $n_{\rm H} = 5 \times 10^6$ and 5×10^8 cm^{-3}, respectively. However, as it is seen for the strong luminosity outburst case, the freeze-out timescale decreases with the density to become much shorter than the outburst timescale for a high density of 5×10^8 cm^{-3}. As a consequence, methanol freezes-out efficiently before the onset of the MF and DME recondensations and their abundance ratios strongly increase as the methanol decreases, reaching the similar high abundance ratios as for the strong luminosity outburst case.

Other parameters can also affect the formation and the freeze-out efficiencies of COMs and methanol, altering the evolution of their abundance. The outburst timescale or the grain size would influence the abundances ratios in a similar manner as for the strong luminosity outburst case. The

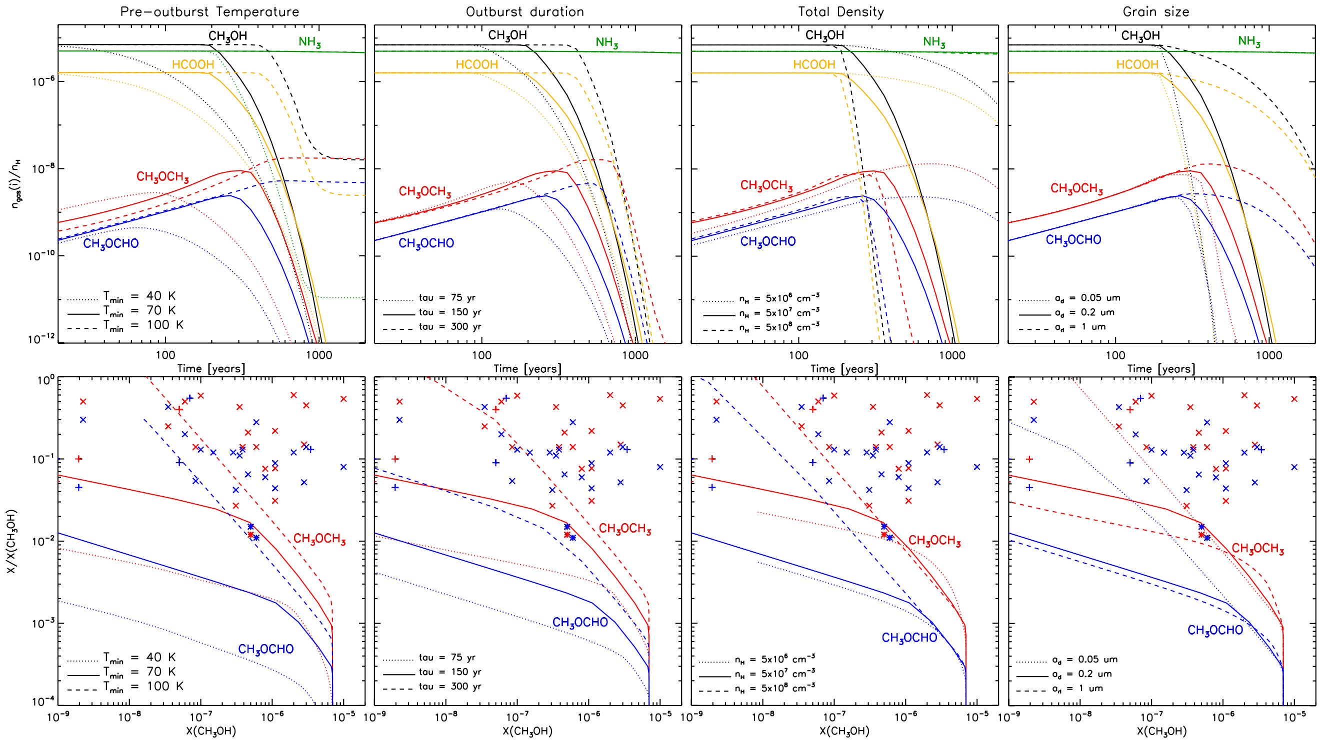

FIG. 6.— Evolution of the absolute abundances of methanol, ammonia, formic acid, di-methyl ether and methyl formate with time (top panels) and of the CH_3OCH_3/CH_3OH (red) and CH_3OCHO/CH_3OH (blue) abundance ratios with the absolute CH_3OH abundance (bottom panels) during one strong luminosity outburst. Pluses, stars, and crosses represent the ratios observed toward low-mass, intermediate-mass, and high-mass protostars, respectively, summarised in Taquet et al. (2015). Left, middle-left, middle-right and right panels show the influence of the pre-outburst temperature $T_{\rm min}$, the luminosity outburst timescale τ, the total density $n_{\rm H}$, and the grain size $a_{\rm d}$ respectively, on the chemistry.

frequency of outbursts is also important for the formation of daughter COMs through gas phase chemistry. More frequent outbursts would reinject solid methanol before NH_3 is efficiently destroyed by gas phase chemistry. If the ammonia abundance is initially similar to methanol, an increase of the outburst frequency would tend to increase the formation efficiency of COMs.

5. DISCUSSION

5.1. *Comparison with observed abundance ratios*

Gas phase chemistry can produce a large amount of complex organics and in particular of DME and MF, the two prototype COMs that have been extensively targeted in hot cores, when proton-transfer reactions involving ammonia are included . In Figure 4, observational data obtained toward more than 40 low-mass to high-mass protostars, are shown together with the predictions of our static model. The observational data has been compiled in Taquet et al. (2015), and is complemented by the recent detections of ethyl formate toward Sgr B2 by Belloche et al. (2009) and of ethyl formate and methyl ethyl ether toward Orion KL by Tercero et al. (2015). The comparison with observations suggests that gas phase chemistry with constant physical conditions is able to explain the abundance of DME and MF with respect to methanol toward some of the methanol-enriched protostars, with methanol abundances higher than 10^{-6}, that show abundance ratios between 2 and 20 %. However, the abundance ratios higher than 20 % cannot be reproduced with our static gas phase model.

Grain surface chemistry, in which COMs are formed from the UV-induced radical recombination on warm ($30 \leq T \leq 80$ K) interstellar grains has been recently proposed to explain the detection of DME, MF and other COMs around protostars (see Garrod & Herbst 2006; Garrod et al. 2008). However, these gas-grain astrochemical models still strongly underpredict the abundances of DME and MF with respect to methanol by more than one order of magnitude, the abundance ratios barely exceeding 1 % for the two species, suggesting that other chemical processes, such as gas phase chemistry, would play a major role for the formation of these two species (see Taquet et al. 2015, for a more detailed comparison between observations and models) . In gas-grain models, complex organic molecules, assumed to be mostly formed on interstellar grains, are then evaporated into the gas phase when the temperature exceeds ~ 100 K and are gradually destroyed by gas phase chemistry, through protonation followed by dissociative electronic recombination. The incorporation of gas phase proton transfer reactions involving NH_3 in gas-grain models would delay the destruction of COMs in the gas phase, and increase their absolute abundances in hot cores and hot corinos, as non-dissociative PT reactions would dominate over the dissociative ER reactions. However, it is unlikely that the abundance ratios of these complex species with respect to methanol will be increased since COMs and methanol show similar proton affinities, inducing a similar chemistry. In particular, the abundance of methyl formate with respect to its isomer glycolaldehyde CH_2OHCHO has been found to be higher than 10 in three low-mass protostars (Jørgensen et al. 2012; Coutens et al. 2015; Taquet et al. 2015), contradicting the gas-grain model predictions of Garrod (2013), in which the two molecules are assumed to form on grains from a similar mechanism, with an abundance ratio of ~ 0.1. Methyl formate and glycolaldehyde have a similar proton affinity of 782 kJ/mol, proton transfer reactions cannot be invoked to ex-

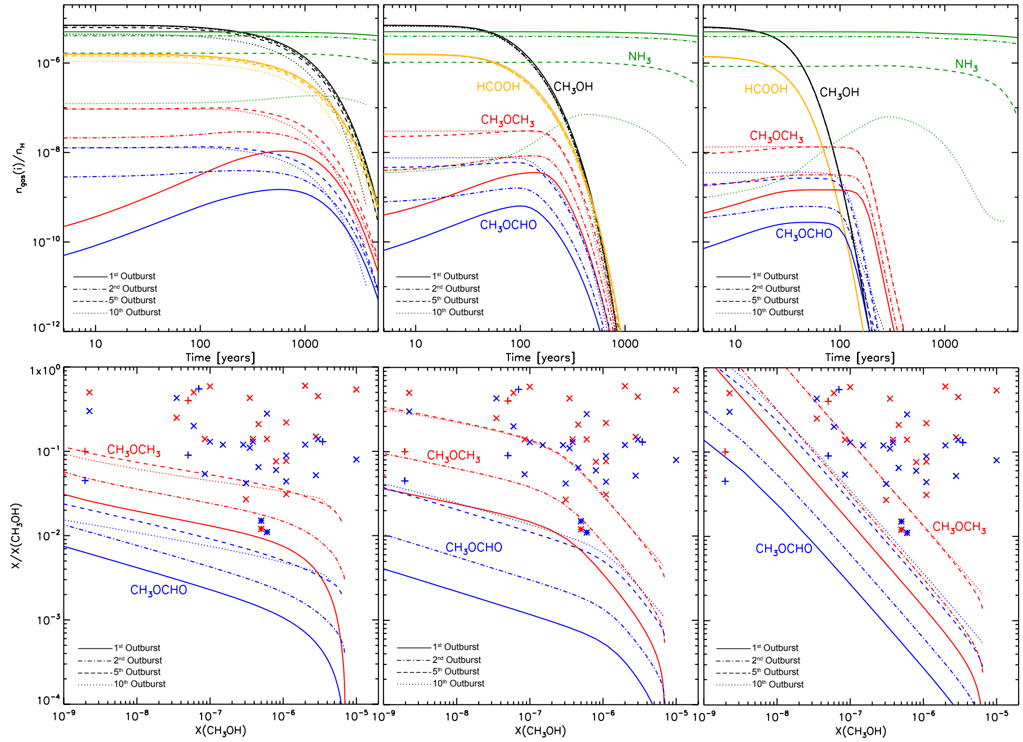

FIG. 7.— Evolution of the absolute abundances of methanol, ammonia, formic acid, ethanol, di-methyl ether and methyl formate with time after the onset of each outburst (top panels) and of the CH_3OCH_3/CH_3OH (red) and CH_3OCHO/CH_3OH (blue) abundance ratios with the absolute CH_3OH abundance (bottom panels) during a series of 10 weak luminosity outbursts occurring every 5×10^3 yr assuming $n_{\rm H} = 5 \times 10^6$ cm^{-3} (left), $n_{\rm H} = 5 \times 10^7$ cm^{-3} (center), and $n_{\rm H} = 5 \times 10^8$ cm^{-3} (right). The thickness of the lines increases with the outburst number: the DME and MF abundances increase with the outburst number while the ammonia abundance decreases. Pluses, stars, and crosses represent the ratios observed toward low-mass, intermediate-mass, and high-mass protostars, respectively, summarised in Taquet et al. (2015).

plain the different abundance ratios. As no efficient gas phase formation routes are known for glycolaldehyde, additional gas phase chemical pathways leading to the formation of methyl formate naturally explain the high abundance of methyl formate with respect to its isomer.

The abundance ratios of ethyl formate and methyl ethyl ether of 10^{-3} observed toward Sgr B2 and Orion KL can also be reproduced by the gas phase chemistry depicted in Fig. 2 triggered by the evaporation of the solid methanol, ethanol, and formic acid, depending on the assumed physical conditions and initial abundances. The high proton affinity of ethanol C_2H_5OH can explain the lower abundances of $1 - 10$ % relative to methanol observed in the gas phase of hot cores with respect to the initial abundance of 23 % in ices assumed in this work. However, due to its low proton affinity, the predicted abundance ratio of HCOOH slightly increases with time and overpredicts the hot core observations by one to two orders of magnitude. The discrepancy between the model predictions and the observations could be due to an overprediction by the models induced by a overestimation of the initial abundance of HCOOH, or by some missing destruction channels for gaseous HCOOH. However, it should be noted that the HCOOH abundances derived from observations in hot cores are only based on the detection of its more stable *trans* conformer. Laboratory experiments studying the formation of solid CO_2 and HCOOH through the CO+OH reaction show that the HOCO complex, thought to act as an intermediate for the formation of both products, can be formed in its two *trans*- and *cis*- conformers in similar quantities (Oba et al. 2010; Ioppolo et al. 2011). Moreover, *cis*-HCOOH has recently been detected in a molecular cloud with a similar abundance than the *trans* counterpart (Taquet et al. in prep.) suggesting that the observed abundance ratios of HCOOH are likely underestimated.

Due to its high proton affinity, ammonia can abstract a proton from most of the ions through proton-transfer reactions, altering the protonation of methanol and the formation of neutral complex organic molecules from their protonated counterpart. As shown in section 3.2 and Fig. 5, the abundance ratios of COMs highly depend on the initial abundance of ammonia and reach their maximum at ammonia abundances of $5-10$ % with respect to water, when the ammonia abundance is similar to methanol. These abundances are in agreement with the typical icy ammonia abundances of 0.6-1.4 and 1.3-2.0 relative to solid methanol observed toward low-mass and high-mass protostars respectively (Öberg et al. 2011). Gas phase abundances of NH_3 and CH_3OH should also remain similar as long as the timescale is not longer than $\sim 10^5$ yr (see Fig. 1). We have attempted to derive the NH_3/CH_3OH abundance ratios toward 9 high-mass hot cores showing a detection of ammonia and methanol. For all sources, the NH_3/CH_3OH abundance ratio was derived following the published NH_3 and CH_3OH column densities and scaled according to the size of their emission. We found the following NH_3/CH_3OH abundance ratios: 0.38 in G19.61-0.23 (Qin et al. 2010), 0.37 in G24.78 (Codella et al. 1997; Bisschop et al. 2007), 4.3 in G29.96 (Cesaroni et al. 1994; Beuther et al. 2007b), 6.8 in G31.41+0.31 (Cesaroni et al. 1994; Isokoski et al. 2013), 0.63 in NGC6334-I-mm1 and 0.32 in NGC6334-I-mm2 (Beuther et al. 2007a; Zernickel 2015), 2.5 in NGC7538IRS1 (Bisschop et al. 2007; Goddi et al. 2015), 0.60 in the "Hot Core" in Orion KL (Goddi et al. 2011; Feng et al. 2015), and

0.098 in W33A (Bisschop et al. 2007; Lu et al. 2014). Due to the low number of sources, no trend for the evolution of the abundance ratio with the methanol abundance can be noticed but we derived an averaged NH_3/CH_3OH abundance ratio of 1.8, in good agreement with the values found in interstellar ices toward high-mass protostars. The similar abundance of ammonia and methanol found in ices and in the gas phase suggests that gas phase does not destroy more efficiently ammonia than methanol in the early stages of star formation.

This work focused on the gas phase chemistry triggered by the evaporation of interstellar ices. The chemical composition of ices was therefore taken from infrared observations. It is known that several species like methanol can show a large variation of their abundances with respect to water depending on the source (Öberg et al. 2011) while the presence of formic acid and ethanol in ices inferred from the band at 7.25 μm, and their exact abundance, is still a matter of debate. The gas phase formation of complex organic molecules obviously depends on the initial abundance of the parent species, the absolute abundance of dimethyl ether, methyl formate, and other larger species linearly scales with the initial amount of methanol, formic acid, and ethanol injected in the gas. The variation of methanol abundance does not strongly alter the abundance ratios of the studied COMs, as long as the abundances of ethanol, formic acid, and ammonia are scaled to methanol. However,for a fixed abundance of methanol, the abundances of methyl formate, ethyl formate, or methyl ethyl ether tend to vary almost linearly with the initial abundances of ethanol and formic acid assumed in the ices. The high sensitivity and spectral resolution provided by new generations of infrared telescopes, such as the James Webb Space Telescope (JWST), together with new laboratory experiments focusing on the absorption infrared spectra of complex species are therefore required to confirm the presence of ethanol and formic acid in the quantities assumed in this work.

We assumed a branching ratio of 100 % for reaction (4) forming *trans*-protonated MF following the suggestion by Cole et al. (2012) (see section 2.2) and for the PT reaction between *trans*-protonated MF and ammonia, producing *cis*-MF, in the absence of quantitative data and based on the energy differences between *cis*- and *trans*-MF. These branching ratios might be too optimistic and new laboratory work are needed to confirm or infirm these assumptions. Lowering the branching ratio of these reactions to 10 % decreases the maximal abundance ratio of methyl formate with respect to methanol by a factor of 2.5 from 4 % to 1.5 % when standard input parameters are assumed.

5.2. *Impact of luminosity outbursts*

The distribution of bolometric luminosities of embedded protostars derived by infrared surveys show that most low-mass protostars have relatively low-luminosities of about $1 - 5L_\odot$ (Evans et al. 2009). For such low-luminosity sources, the water snow line is located only 10-20 AU away from the central source (or ~ 0.1 arcsec at a typical distance of 200 pc), making the detection of complex organic molecules in hot cores with current sub-mm facilities very challenging, even with ALMA. However, in spite of their short timescale of ~ 100 years, luminosity outbursts are able to produce COMs through gas phase chemistry in significant quantities, with absolute abundances higher than 10^{-8} in large regions outside the hot core up to 50 to 200 AU away from the central source, depending on the strength of the luminosity outbursts and the structure of the protostellar envelope.

Due to their low binding energies, the abundances of COMs formed either at the surface of interstellar grains or in the gas phase relative to methanol tend to increase after each luminosity outburst as the methanol decreases. In the inner regions of protostellar envelopes, the density varies between 10^6 and 10^{10} cm^{-3} depending on the distance from the protostar and the source in consideration. Low-density sources would display high absolute abundances of methanol and COMs long after the luminosity outburst ends due to their slow freeze-out. At a density of 5×10^6 cm^{-3}, the freeze-out timescale becomes similar to the timescale between outbursts (1000 - 5000 yr depending on the assumed grain size, see equation 5), methanol and COMs can therefore remain in the gas phase in a large region of the protostellar envelope during most of the embedded stage. However, the abundance ratios of COMs would remain limited because methanol and COMs deplete simultaneously, the abundance ratios after outbursts do not exceed 5 %. On the other hand, dense protostars that underwent recent outburst events would likely display a low methanol abundance in the region just outside of the expected water snow line, due to its fast freeze-out onto grains, associated with a high abundance ratio of COMs, induced by their lower binding energy, that could match the observed abundance ratios. According to Fig. 6, the methanol abundance stays higher than 10^{-10} for about 500 yr. Assuming that outburst events occur every $5 \times 10^3 - 10^4$ yr (Scholz et al. 2013; Vorobyov et al. 2015) suggests that an extended emission of COMs could be detected with high abundance ratios in about $5 - 10$ % of dense protostars.

Other species that show lower binding energies and which also likely undergo similar behaviours during the recondensation process occurring after luminosity outbursts can be used to identify chemical clocks for episodic phenomena. By performing SMA observations of the $C^{18}O$ emission around a sample of 16 well-characterised protostars, Jørgensen et al. (2015) found that half of them show extended $C^{18}O$ emission compared to the $C^{18}O$ emission expected from their current luminosities. This discrepancy can be attributed to previous outburst events increasing the luminosity by a factor of five or more during the last 10^4 yr, and even by a factor of 25 for 25 % of the observed sources. High-angular resolution observations, using the new generation of sub-mm interferometers like ALMA, of such sources will be crucial for testing the gas phase chemistry scenario proposed in this work. Depending on the density structure of these sources, the emission of methanol and COMs could eventually be also extended with respect to the hot core region expected from their current luminosity. Comparison of their emission and their abundance inside and outside the expected hot core region will help us assessing whether or not luminosity outbursts can trigger the formation of COMs and alter their observed abundance ratios.

6. CONCLUSIONS

In this work, we have investigated the gas phase formation and evolution of complex organic molecules (COMs) for constant physical hot core conditions and during protostellar luminosity outbursts. We summarise here the main conclusions of this work:

1) Ion-neutral gas phase chemistry, triggered by the evaporation of interstellar ices at temperatures higher than 100 K, can efficiently produce several complex organic molecules. The incorporation of proton-transfer reactions involving ammonia, in which its high proton affinity plays a crucial role,

results in an efficient formation and a delayed destruction of complex organic molecules. The initial abundance of ammonia injected in the gas phase is found to be the most important parameter for the production of complex organic molecules. These results, in addition to the recent works by Vasyunin & Herbst (2013) and Balucani et al. (2015) who proposed new gas phase neutral-neutral reaction routes, suggest a gas phase origin for several complex organic molecules.

2) Comparison with observations suggests that gas phase chemistry occurring during constant physical conditions can account for the abundances of di-methyl ether and methyl formate, the two bright and abundant COMs, relative to methanol in almost half of the observed protostars without recourse to grain surface chemistry. In addition, the abundance ratios of the more complex species ethyl formate and ethyl methyl ether observed in Orion KL and Sgr B2 can also be reproduced with our gas phase chemical network. However, as the gas phase formation of complex organic molecules highly depends on the initial abundance of solid species, like HCOOH and C_2H_5OH and the branching ratios of some ion-neutral reactions, which are still a matter of debate, more laboratory and observational works using new generations of telescopes are needed to confirm these results.

3) In spite of their short timescales, one strong protostellar luminosity outburst or a series of five weak outburst events can produce complex organic molecules in appreciable amounts through gas phase chemistry in a large region of protostellar envelopes. Di-methyl ether and methyl formate, for example, can be produced with absolute abundances of about 10^{-8} in protostellar envelope regions with sizes increasing by a factor of 5 to 10, depending on the strength of the luminosity outburst, with respect to the pre-outburst hot core.

4) Because of their lower binding energy that delays their recondensation, the abundances of di-methyl ether and methyl formate relative to methanol tend to increase during the cooling occurring after the outburst, especially when high total densities or low interstellar grain sizes are assumed.

5) The high abundances of di-methyl ether and methyl formate of ~ 50 % observed toward some of the observed protostars could be explained by previous recent luminosity outburst events that trigger the formation of these molecules in a large region of the envelope followed by by a delayed recondensation onto grains with respect to methanol.

We thank the anonymous referee for his/her insightful comments that helped to improve the quality of the manuscript. V.T. acknowledges the support from the NASA postdoctoral program. E.S.W. acknowledges generous financial support from the Swedish National Space Board. S.B.C. was supported by NASA's Origins of Solar Systems Program.

REFERENCES

Ábrahám, P., Kóspál, Á., Csizmadia, S., Kun, M., Moór, A. and Prusti, T. 2004, A&A, 428, 89-97
Acharyya, K., Fuchs, G. W., Fraser, H. J., van Dishoeck, E. F. and Linnartz, H. 2007, A&A, 466, 1005-1012
Anicich, V. G. 1993, ApJS, 84, 215-315
Audard, M., Ábrahám, P., Dunham, M. M. et al. 2014, Protostars and Planets VI, 387-410
Avgul, N. N. and Kiselev, A. V. 1970, Chem. Phys. Carbon, 6, 1
Balucani, N., Ceccarelli, C. and Taquet, V. 2015, MNRAS, 449, L16
Belloche, A., Garrod, R. T., Müller, H. S. P. et al. 2009, A&A, 499, 215
Bell, K. R. and Lin, D. N. C. 1994, ApJ, 427, 987-1004
Beuther, H., Walsh, A. J., Thorwirth, S. et al. 2007, A&A, 466, 989
Beuther, H., Zhang, Q., Bergin, E. A. et al. 2007, A&A, 468, 1045
Bisschop, S. E., Fraser, H. J., Öberg, K. I., van Dishoeck, E. F. and Schlemmer, S. 2006, A&A, 449, 1297-1309
Bisschop, S. E., Jørgensen, J. K., van Dishoeck, E. F., and de Wachter, E. B. M. 2007, A&A, 465, 913-929
Blake, G. A., Sutton, E. C., Masson, C. R. and Phillips, T. G. 1987, ApJ, 315, 621-645
Boogert, A. C. A., Pontoppidan, K. M., Knez, C., Lahuis, F. et al. 2008, ApJ, 678, 985-1004
Bottinelli, S., Boogert, A. C. A., Bouwman, J., Beckwith, M. et al. 2010, ApJ, 718, 1100
Brown, W. A. and Bolina, A. S. 2009, MNRAS, 374, 1006-1014
Cazaux, S., Tielens, A. G. G. M., Ceccarelli, C., Castets, A., Wakelam, V., Caux, E., Parise, B. and Teyssier, D. 2003, ApJ, 593, L51-L55
Cesaroni, R., Churchwell, E., Hofner, P., Walmsley, C. M. and Kurtz, S. 1994, A&A, 288, 903
Charnley, S. B., Kress, M. E., Tielens, A. G. G. M. and Millar, T. J. 1995, ApJ, 448, 232
Codella, C., Testi, L. and Cesaroni, R. 1997, A&A, 325, 282
Cole, C. A., Wehres, N., Yang, Z. et al. 2012, ApJ, 754, L5
Collings, M. P., Anderson, M. A., Chen, R., Dever, J. W., Viti, S., Williams, D. A. and McCoustra, M. R. S. 2004, MNRAS, 354, 1133-1140
Coutens, A., Persson, M. V., Jørgensen, J. K., Wampfler, S. F. and Lykke, J. M. 2015, A&A, 576, A5
Dartois, E., Schutte, W., Geballe, T. R., Demyk, K., Ehrenfreund, P. and D'Hendecourt, L. 1999, A&A, 342, L32-L35
Dunham, M. M. and Vorobyov, E. I. 2012, ApJ, 747, 52
Ehrenfreund, P. and Charnley, S. B. 2000, ARA&A, 38, 427-483
Evans, II, N. J., Dunham, M. M., Jørgensen, J. K., Enoch, M. L., Merín, B., van Dishoeck, E. F., Alcalá, J. M., Myers, P. C., Stapelfeldt, K. R., Huard, T. L., Allen, L. E., Harvey, P. M., van Kempen, T., Blake, G. A., Koerner, D. W., Mundy, L. G., Padgett, D. L. and Sargent, A. I. 2009, ApJS, 181, 321-350
Feng, W. Y. and Lifshitz, C. 1994, The Journal of Physical Chemistry, 98, 3658-3663
Feng, S., Beuther, H., Henning, T., Semenov, D., Palau, A. and Mills, E. A. C. 2015, A&A, 581, A71
Fraser, H. J., Collings, M. P., McCoustra, M. R. S. and Williams, D. A. 2001, MNRAS, 327, 1165-1172
Garrod, R. T., and Herbst, E. 2006, ApJ, 936, 13
Garrod, R. T., Weaver, S. L. W. and Herbst, E. 2008, ApJ, 682, 283-302
Garrod, R. T. 2013, ApJ, 765, 60
Geppert, W. D., Hamberg, M., Thomas, R. D. et al. 2006, Faraday Discussions, 133, 177
Gibb, E. L., Whittet, D. C. B., Boogert, A. C. A. and Tielens, A. G. G. M. 2004, ApJS, 151, 35
Goddi, C., Greenhill, L. J., Humphreys, E. M. L. et al. 2011, ApJ, 739, L13
Goddi, C., Zhang, Q. and Moscadelli, L. 2015, A&A, 573, A108
Gramajo, L. V., Rodón, J. A. and Gómez, M. 2014, AJ, 147, 140
Hamberg, M., Österdahl, F., Thomas, R. D. et al. 2010, A&A, 514, A83
Hamberg, M., Zhaunerchyk, V., Vigren, E. et al. 2010, A&A, 522, A90
Herbst, E. and van Dishoeck, E. F. 2009, ARA&A, 47, 427-480
Hemsworth, R. S., Payzant, J. D., Schiff, H. I. and Bohme, D. K. 1974, Chemical Physics Letters, 26, 417-421
Herrero, V. J., Galvez, O., Maté, B. and Escribano, R. 2010, Phys. Chem. Chem. Phys., 12, 3164-3170
Horn, A., Møllendal, H., Sekiguchi, O., Uggerud, E., Roberts, H., Herbst, E., Viggiano, A. A., and Fridgen, T. D. 2004, ApJ, 611, 605-614
Huntress, Jr., W. T. 1977, ApJS, 33, 495-514
Ioppolo, S., Cuppen, H. M., van Dishoeck, E. F. and Linnartz, H. 2011, MNRAS, 410, 1089
Isokoski, K., Bottinelli, S. and van Dishoeck, E. F. 2013, A&A, 554, A100
Ivezic, Z. and Elitzur, M. 1997, MNRAS, 287, 799-811
Johnstone, D., Hendricks, B., Herczeg, J. and Bruderer, S. 2013, ApJ, 765, 133
Jørgensen, J. K., Favre, C., Bisschop, S. E. et al. 2012, ApJ, 757, L4
Jørgensen, J. K., Visser, R., Sakai, N., Bergin, E. A. et al. 2013, ApJ, 779, L22
Jørgensen, J. K., Visser, R., Williams, J. P., Bergin, E. A. 2015, A&A, 579, A23

Karpas, Z. and Meot-Ner, M. 1989, J. Phys. Chem., 93, 1859-1863
Kristensen, L. E., van Dishoeck, E. F., Bergin, E. A., Visser, R., Yıldız, U. A., San Jose-Garcia, I. et al. 2012, A&A, 2012, 542, A8
Lattelais, M., Bertin, M., Mokrane, H., Romanzin, C., Michaut, X., Jeseck, P., Fillion, J.-H., Chaabouni, H. et al. 2011, A&A, 532, A12
Lu, X., Zhang, Q., Liu, H. B., Wang, J. and Gu, Q. 2014, ApJ, 790, 84
Maury, A. J., André, P., Men'shchikov, A., Könyves, V. and Bontemps, S. 2011, A&A, 535, A77
Neill, J. L., Steber, A. L., Muckle, M. T., Zaleski, D. P. et al. 2011, Journal of Physical Chemistry A, 115, 6472-6480
Noble, J. A., Congiu, E., Dulieu, F. and Fraser, H. J. MNRAS, 2012, 421, 768-779
Noble, J. A., Theule, P., Mispelaer, F., Duvernay, F., Danger, G., Congiu, E. and Dulieu, F. and Chiavassa, T. 2012, A&A, 543, A5
Oba, Y., Watanabe, N., Kouchi, A. et al. 2012, ApJ, 712, L174
Öberg, K. I., Garrod, R. T., van Dishoeck, E. F. and Linnartz, H. 2009, A&A, 504, 891-913
Öberg, K. I., Boogert, A. C. A., Pontoppidan, K. M., van den Broek, S., van Dishoeck, E. F., Bottinelli, S., Blake, G. A. and Evans, II, N. J. 2011, ApJ, 740, 109
Pagani, L., Steinacker, J., Bacmann, A., Stutz, A. and Henning, T. 2010, Science, 329, 1622
Pontoppidan, K. M., van Dishoeck, E. F. and Dartois, E. 2004, A&A, 426, 925-940
Qin, S.-L., Wu, Y., Huang, M. et al. 2010, ApJ, 711, 399
Rodgers, S. D. and Charnley, S. B. 2001, ApJ, 546, 324-329
Safron, E. J., Fischer, W. J., Megeath, S. T. et al. 2015, ApJ, 800, L5
Sandford, S. A. and Allamandola, L. J. 1990, ApJ, 355, 357-372
Sandford, S. A. and Allamandola, L. J. 1993, ApJ, 417, 815-825
Scholz, A., Froebrich, D. and Wood, K. 2013, MNRAS, 430, 2910
Smith, D., Spanel, P. and Millar, T. J. 1994, MNRAS, 266, 31
Taquet, V., Ceccarelli, C. and Kahane, C. 2012, A&A, 538, A42
Taquet, V., Charnley, S. B., Sipilä, O. 2014, ApJ, 791, 1
Taquet, V., López-Sepulcre, A., Ceccarelli, C. et al. 2015, ApJ, 804, 81
Tercero, B., Cernicharo, J., López, A. et al. 2015, A&A, 582, L1
Tielens, A. G. G. M., Tokunaga, A. T., Geballe, T. R. and Baas, F. 1991, ApJ, 381, 181-199
Vasyunin, A. I. and Herbst, E. 2013, ApJ, 769, 34
Vigren, E., Hamberg, M., Zhaunerchyk, V. et al. 2010, ApJ, 709, 1429-1434
Visser, R., van Dishoeck, E. F., Doty, S. D. and Dullemond, C. P. 2009, A&A, 495, 881
Visser, R. and Bergin, E. A. 2012, ApJ, 754, L18
Vorobyov, E. I. and Basu, S. 2005, ApJ, 633, L137
Vorobyov, E. I., Baraffe, I., Harries, T. and Chabrier, A&A, 557, A35
Vorobyov, E. I. and Basu, S. 2015, ApJ, 805, 115
Zernickel, A. 2015, PhD thesis
Zhu, Z., Hartmann, L. and Gammie, C. 2009, ApJ, 694, 1045-1055